PAPER • OPEN ACCESS

# P-type silicon as hole supplier for nitride-based UVC LEDs

To cite this article: Sang June Cho *et al* 2019 *New J. Phys.* **21** 023011

New Journal of Physics
The open access journal at the forefront of physics

Deutsche Physikalische Gesellschaft DPG
IOP Institute of Physics

Published in partnership with: Deutsche Physikalische Gesellschaft and the Institute of Physics

OPEN ACCESS

RECEIVED
19 July 2018

REVISED
21 January 2019

ACCEPTED FOR PUBLICATION
4 February 2019

PUBLISHED
28 February 2019



PAPER

# P-type silicon as hole supplier for nitride-based UVC LEDs

**Sang June Cho[1,7], Dong Liu[1,7], Jung-Hun Seo[1,7], Rafael Dalmau[2], Kwangeun Kim[1], Jeongpil Park[1], Jiarui Gong[3], Deyin Zhao[4], Fei Wang[5], Xin Yin[5], Yei Hwan Jung[1], In-Kyu Lee[1], Munho Kim[1], Xudong Wang[5], John D. Albrecht[6,8], Weidong Zhou[4], Baxter Moody[2,8] and Zhenqiang Ma[1,8]**

[1] Department of Electrical and Computer Engineering, University of Wisconsin-Madison, 1415 Engineering Drive, Madison, WI 53706, United States of America
[2] HexaTech, Inc., 991 Aviation Parkway, Suite 800, Morrisville, NC 27560, United States of America
[3] Department of Physics, University of Wisconsin-Madison, 1415 Engineering Drive, Madison, WI 53706, United States of America
[4] Department of Electrical Engineering, University of Texas at Arlington, 500 South Cooper Street, Arlington, TX 76019, United States of America
[5] Department of Materials Science and Engineering, University of Wisconsin-Madison, Madison, 1509 University Avenue, Madison, WI 53706, United States of America
[6] Department of Electrical and Computer Engineering, Michigan State University, 428S. Shaw Lane, East Lansing, MI 48824, United States of America
[7] Authors contributed equally.
[8] Authors to whom any correspondence should be addressed.

**E-mail: jalbrech@egr.msu.edu, bmoody@hexatechinc.com and mazq@engr.wisc.edu**

**Keywords:** tunneling, single crystal nanomembrane, atomic layer deposition, transfer printing, hole injector, light emitting diodes

Supplementary material for this article is available online

## Abstract

The ineffective p-type doping of nitrides using magnesium (Mg), the best available dopant, has limited the development and performance of all III-nitride-based devices, including bipolar junction transistors and light emitting diodes (LEDs). For nitride-based ultraviolet (UV) LEDs, as the Al composition increases for achieving shorter wavelengths (e.g. <280 nm) into the UVC spectral range, the p-type doping issue, which causes very inefficient hole injection, becomes more severe than ever. In this work, we report the detailed study of using p-type Si as a hole supplier for high-Al composition UVC LEDs. We first describe the method of Si/GaN junction formation, where the lattice-mismatch challenge between Si and GaN is overcome by using a 0.5 nm thick $Al_2O_3$ layer at the interface. This serves as a physical separation layer between the two materials as well as a passivation, tunneling, and thermal buffer layer. High-resolution transmission electron microscope image illustrates the high-quality interface between Si and GaN. We further detail the hole transport mechanism of the p–p Si/GaN isotype junction through both simulations and experiments. The enhanced hole concentration in the AlGaN/AlN multiple quantum wells (MQWs) due to the use of p-type Si as the hole supplier is verified through comparison with conventional UVC LEDs. Finally, high-performance UVC LEDs made with AlN/AlGaN (Al: 72%) MQWs employing p-type Si as their hole suppliers are demonstrated experimentally to serve as an example of the novel hole injector strategy.

## 1. Introduction

A fundamental limitation of III-nitride materials, particularly the nitrides with a high Al content, for junction type devices (e.g. light emitting diodes (LEDs) and bipolar junction transistors) is their ineffective p-type doping. Using magnesium (Mg), the best p-type dopant, to dope GaN, the highest available free hole concentration can reach the low 18th order due to the high ionization energy of Mg in GaN (0.2–0.15 eV for the Mg concentration between $1 \times 10^{19}$ and $5 \times 10^{19}$ $cm^{-3}$) [1]. Such a hole concentration has enabled high-efficiency blue LEDs. However, the even higher ionization energy of Mg in AlGaN leads to a much lower hole concentration than the 18th order in p-type AlGaN. The ineffective p-type doping in AlGaN has severely hindered the development of AlGaN-based ultraviolet (UV) LEDs. A higher Al composition in AlGaN for shorter UV wavelengths would

result in a higher ionization energy of Mg (e.g. ~0.5 eV for AlN:Mg) [2–4] At present, all AlGaN-based LEDs employ p-type GaN as their hole injector. The thickness of the p-type GaN is typically 100–200 nm thick as needed for a p-type contact layer. Due to the lattice mismatch between GaN and AlGaN, the quality p-type GaN is often degraded, which further decreases the hole concentration in p-type GaN. On the other hand, n-type nitrides can reach a fairly high electron concentration level (close to 19th order), leading to a severe imbalance between the electron and hole concentrations within the active region [5]. The insufficient hole supply for III-nitrides contributes to the poor performance of LEDs made therefrom.

To improve the free hole concentration in high-Al content AlGaN materials, researchers have developed the approach of polarization doping [6–10] for the purpose of enhancing electrical conductivity. By linearly grading the Al composition of AlGaN, the polarization bound charge spreads to a 3D form and induces the formation of a mobile 3D carrier gas of the opposite charge, resulting in an increased carrier concentration [11–15] over impurity doping. However, to produce substantial effective doping, there must be a strong composition gradient (a large range of Al:Ga ratio). This capability diminishes as the Al composition in AlGaN quantum wells approaches the binary endpoint, AlN, which is necessary to generate high energy photons. Another method to improve the hole concentration requires the use of nanowires [16] where high strain can be accommodated in p-type GaN such that an improved fraction of Mg ionization in GaN is expected. Nevertheless, all these methods are incremental measures to improve the free hole concentrations in the quantum wells of UV LEDs.

In this paper, we describe a novel measure to substantially increase the hole concentration in nitride-based multiple quantum wells (MQWs). Instead of using Mg-doped nitride as the hole supplier, we used p-type Si for nitride-based MQWs. Since Si can be heavily doped (20th–21st order) into p-type Si using boron atoms, for which the ionization energy of boron is in the level of thermal energy, even if partial (e.g. ~10%) free holes in Si can be injected into the nitride-based MQWs, the imbalance between electron and hole concentrations in the MQWs could be greatly improved. However, the epitaxy of GaN on Si is challenging mainly due to a remarkable lattice mismatch. Si (111) plane is commonly chosen due to its trigonal symmetry facilitating a hexagonal Wurtzite structure. Due to lattice parameter differences, i.e. 0.3823 nm for Si (111) versus 0.3112 nm for AlN (0001) (or 0.3189 nm for GaN (0001)), the interface density of states can be very high with epitaxial growth [17]. The extensive practice of direct wafer bonding between two materials, which leads to poor interface quality with a very high density of interface states, has also proven to be infeasible for forming Si/GaN junctions of needed quality [18].

To solve the lattice mismatch challenge, we employed the ultrathin oxide interfaced heterostructure method [19, 20] to realize the Si/III-nitride isotype heterojunction. By inserting a layer of ultrathin oxide in between two semiconductors of any sized lattice constants, the two semiconductors are physically separated. As a result, interface defects due to lattice mismatch and/or crystal disorientation, as happens in wafer bonding, can be avoided. Without the concern of lattice mismatch, Si [100] was adopted based on the SOI material availability. The oxide type was selected such that it could effectively passivate the surfaces of the two semiconductors. If the oxide is sufficiently thin, it will serve as a quantum tunneling layer that allows the passage of both electrons and holes. The thickness of the oxide was determined by satisfying the requirements of both the surface passivation and efficient quantum tunneling. Practically, for a p–n diode fabricated using the heterostructure method, the influence of the oxide thickness is reflected on the diode ideality factor, rectification ratio, and reverse breakdown characteristics. With an optimum thickness of the oxide, ideal p–n diodes are readily achievable [20]. Since most oxides have plasticity at certain elevated temperatures, the oxides can serve as a thermal buffer layer that eases the bonding of the two semiconductors during chemical bonding to form the heterostructure.

The abovementioned heterostructure method is supposed to provide a universal scheme to form ideal abrupt junctions between dissimilar bulk (3D) semiconductors with minimum interface density of states. Nevertheless, application of the unique lattice-mismatched heterostructure method to solve the poor p-type doping challenges of III-nitrides has been very limited [21].

In this study, we formed a p-type Si/p-type GaN junction to enable the p-type Si as a hole injector. Heavily p-type doped Si nanomembrane (NM) was released from silicon-on-insulator (SOI), transferred and chemically bonded via rapid thermal anneal (RTA) to a p-type GaN layer that was first coated with a 0.5 nm thick $Al_2O_3$ layer using atomic layer deposition (ALD). $Al_2O_3$ is already well-known to be able to passivate both Si [22, 23] and GaN [24, 25] effectively. The 0.5 nm thickness of the ALD $Al_2O_3$ layer was decided based on the best measured current density–voltage characteristics of p-Si/$Al_2O_3$/p-GaN heterostructures. High-resolution transmission electron microscopy (HRTEM) was used to reveal the detailed lattice structure of the Si/$Al_2O_3$/GaN interface. The electrical conductivity and band alignment of the p-type Si/GaN isotype junction were experimentally examined via current–voltage ($I$–$V$) and capacitance–voltage ($C$–$V$) characterizations. The calculated band alignment information was then used to examine the hole injection condition into AlGaN/AlN MQWs via simulations. Finally, UVC LEDs sequentially consisting of 100 nm transferred p-type Si, 0.5 nm ALD $Al_2O_3$, and an epitaxially grown structure including 20 nm p-GaN, 2 nm $Al_{0.72}Ga_{0.28}N$/ 6 nm AlN x3 MQWs,

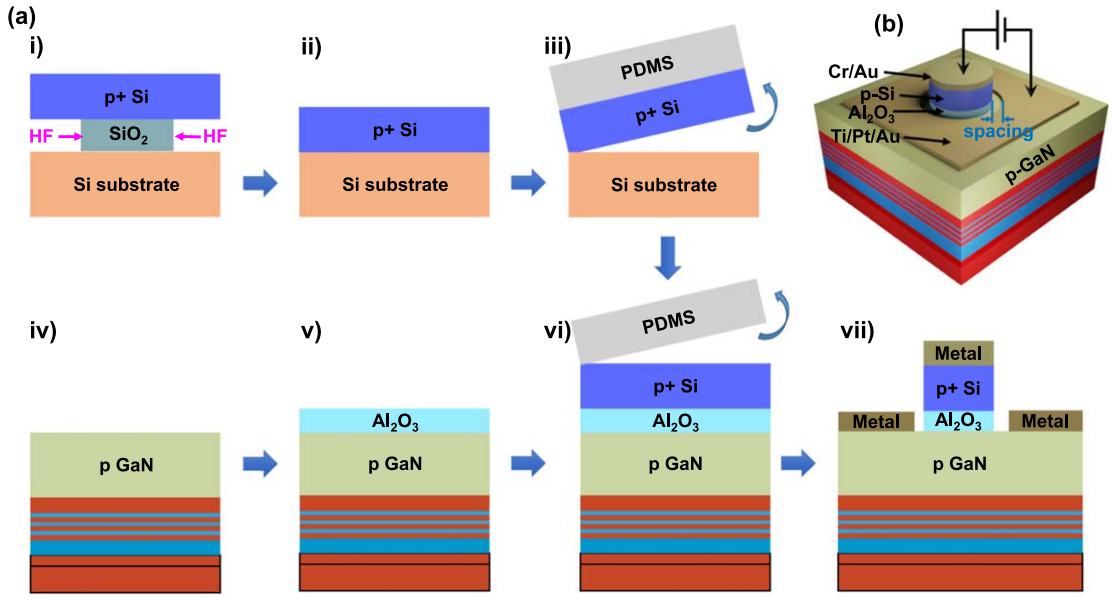


**Figure 1.** Formation of $Al_2O_3$-interfaced Si/GaN junction. (a) Schematic illustration of the fabrication process flow. (i)–(ii). A heavily boron doped ($5 \times 10^{19}$ $cm^{-3}$) SOI substrate was used to create single-crystalline Si NM of 100 nm thick by sacrificially etching away the buried oxide using hydrofluoric acid. (iii) Pick up the released Si NM using a polydimethylsiloxane (PDMS) stamp. (iv)–(v) A 0.5 nm thick $Al_2O_3$ layer was deposited using ALD on a 200 nm thick p-type GaN layer that was grown on an MQWs LED epitaxial structure. (vi) The Si NM was transferred to the $Al_2O_3$-coated GaN using the PDMS stamp and a thermal anneal was applied to form chemical bonding. (vii) Metal electrodes were formed on the Si and GaN surface via photolithography. (b) A 3D illustration of the metalized p-Si/$Al_2O_3$/p-GaN heterojunction.

and 600 nm n-type $Al_{0.74}Ga_{0.26}N$ on an AlN substrate were demonstrated with high performance to prove the practicality of using p-type Si as an efficient hole supplier.

## 2. Results and discussion

### 2.1. Si/GaN heterojunction formation

Figure 1(a)(i–vi) illustrates the $Al_2O_3$-interfaced Si/GaN junction formation method and fabrication process flow. In brief, a 0.5 nm thick $Al_2O_3$ layer was deposited using ALD on a 200 nm thick p-type GaN layer that was grown on an MQWs LED (the detail of the LED structure is depicted later) epitaxial structure. A heavily boron doped ($5 \times 10^{19}$ $cm^{-3}$) SOI substrate was used to create single-crystalline Si NM of 100 nm by sacrificially etching away the buried oxide using hydrofluoric acid. The released p-type Si NM was transferred to the $Al_2O_3$-coated GaN and later a chemical bonding was formed via thermal anneal. To characterize the heterostructure for *I–V* and *C–V* characteristics, metal electrodes were formed on the Si and GaN (figure 1(a)(vii)), respectively. Figure 1(b) shows the 3D illustration of the metalized heterostructure.

An HRTEM image of the interface between Si and GaN is shown in figure 2(a), depicting a completed interfacial layer of 0.46–0.99 nm with an average thickness of 0.70 nm. Regardless of the thickness variation, Si and GaN were separated by the $Al_2O_3$ layer. Since ALD deposition can accurately control the thickness of the $Al_2O_3$, the slightly increased interface thickness indicates possible diffusion of $Al_2O_3$ during thermal anneal. The slightly thicker $Al_2O_3$ in some locations than others is presumably due to the surface roughness of Si and GaN. During the RTA procedure, the $Al_2O_3$ has reflowed. From the HRTEM, it can also be seen that the $Al_2O_3$ interfacial layer was partially re-crystallized. While a detailed study is needed to understand the re-crystallization mechanism, it is speculated that a precise alignment during the transfer of Si NM could be partially responsible for the partial re-crystallizations.

### 2.2. Band alignment of p-Si/$Al_2O_3$/p-GaN heterojunction

Despite the high-quality interface between Si and GaN, whether the band alignment between Si and GaN is suitable for hole transport is unknown. Thus, the electrical characteristics of the p-Si/$Al_2O_3$/p-GaN isotype heterojunction were experimentally examined. The *I–V* curves were measured from the p-Si/$Al_2O_3$/p-GaN isotype heterojunction and the data are plotted in linear scale, as shown in figure 2(b). The curves exhibit nearly Ohmic behavior with a very small 'turn-on' voltage. As the spacing between the metal contacts (shown in figure 1(b)) increased from 8 $\mu$m to 10 $\mu$m and 20 $\mu$m, the current decreased for a given voltage, as expected, due

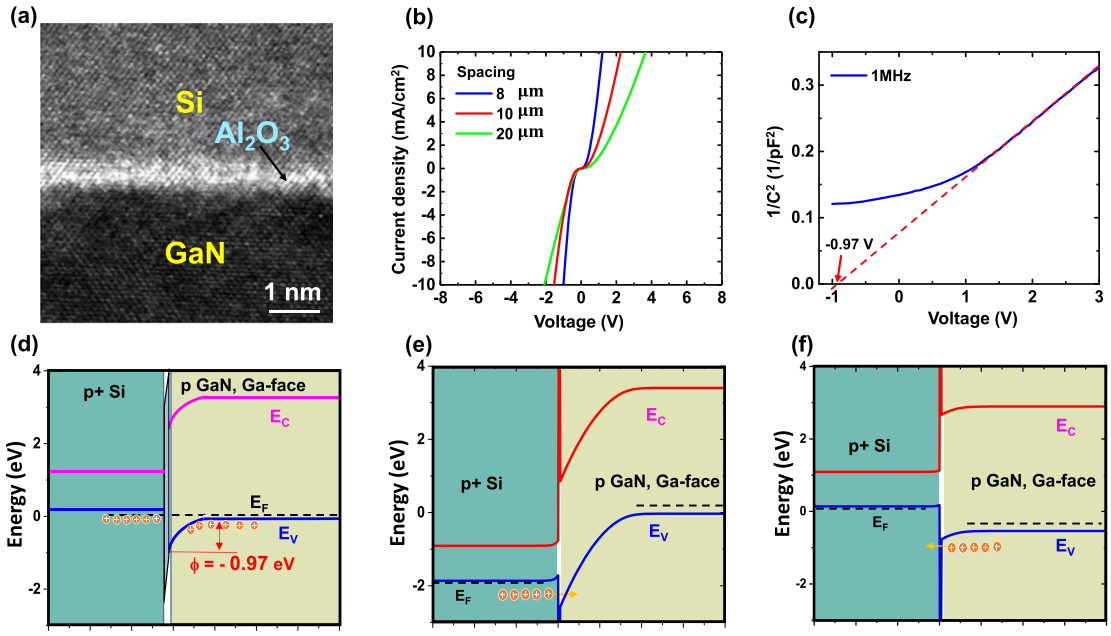


**Figure 2.** Properties of p-type $Si/Al_2O_3$/p-type GaN isotype heterojunction. (a) An HRTEM image of the p-$Si/Al_2O_3$/p-GaN interface. The interface $Al_2O_3$ with nominal thickness of 0.5 nm was slightly broadened and partially re-crystallized. (b) Measured electrical characteristics of the p-$Si/Al_2O_3$/p-GaN heterojunction with different distances between their two metal contacts. (c) Measured $1/C^2$ versus voltage at a frequency of 1 MHz with a 8 $\mu$m gap distance between the two metal contacts. (d) Constructed band diagram of the p-$Si/Al_2O_3$/p-GaN junction under equilibrium. The charge symbols were drawn for holes. (e) and (f) are the band diagrams of the heterojunction under forward bias and reverse bias, respectively.

to the larger lateral current spreading resistance in the p-GaN region. Furthermore, the $C$–$V$ measurements of the p-$Si/Al_2O_3$/p-GaN heterojunction were carried out at a sweeping frequency of 1 MHz. The flat-band voltage was extracted to be −0.97 V from the $1/C^2$–$V$ plot (figure 2(c)), which indicated a built-in potential $\Phi$ of −0.97 eV for the p-$Si/Al_2O_3$/p-GaN heterojunction. Since the free hole concentration of p-Si ($5 \times 10^{19}$ cm$^{-3}$) is more than one order of magnitude higher than that of p-GaN ($\sim 1 \times 10^{18}$ cm$^{-3}$), it is reasonable to assume that the built-in potential mainly originated from the p-GaN (one-sided junction), which was manifested as a 0.97 eV downward band bending of the Ga-polar surface in the p-GaN, as shown in figure 2(d). Additionally, x-ray photoelectron spectroscopy (XPS) was employed to examine the surface/interface of p-GaN with $Al_2O_3$ ALD deposition (figure A1 in the supplementary information (SI) is available online at stacks.iop.org/NJP/21/023011/mmedia), which revealed a downward band bending value of 1.00 eV, consistent with the 0.97 eV band bending value obtained from the $C$–$V$ analysis.

Based on the measurements of the built-in potential, the valence band offset between p-Si and p-GaN can be determined by the following expression [26]:

$$\Phi = \Delta E_v - \delta_{\mathrm{p-Si}} + \delta_{\mathrm{p-GaN}}, \quad (1)$$

where $\Phi$ is the built-in potential, extracted as −0.97 eV. The energy differences, $\delta_{\mathrm{p-Si}}$ and $\delta_{\mathrm{p-GaN}}$, between Fermi levels and valence bands ($E_F$–$E_V$) for heavily doped p-Si and p-GaN (assuming an acceptor ionization ratio of 10% and no strain in GaN) were calculated to be −0.002 eV and 0.12 eV, respectively. Therefore, the valance band offset $|\Delta E_v|$ is 1.092 eV for the p-$Si/Al_2O_3$/p-GaN heterojunction. In comparison to the intrinsic $|\Delta E_v|$ value of 2.32 eV, which can be obtained directly from the electron affinity rule, the energy barrier for hole transport from p-Si to p-GaN was substantially lowered. It is noted that the 20 nm GaN layer should have some strain due to the lattice mismatch between GaN and AlGaN and the strain in GaN (the value is unknown) can change the bandgap of GaN and the band offset values. However, even if a fully strained GaN is considered, the valence band offset value change (estimated to be ∼−0.09 eV) is still too small to undermine the hole injection mechanism. As a result, a much larger concentration of holes can be injected from Si into the MQWs. This difference in energy barrier stems from the negative polarization charges on the surface of the Ga-face GaN, as well as a voltage drop across the interfacial layer induced by the polarization charge. It is also noted that it is the use of the 0.5 nm $Al_2O_3$ interfacial layer, which served as an effective passivation layer for both Si and GaN, that caused the reduced band downward bending of Ga-face GaN (figure A1(c) in the SI), and thus the reduced barrier height for hole transport. Based on the above analyses of the surface band bending and interface-induced valence band offset shift, the band alignment of the p-$Si/Al_2O_3$/p-GaN isotype heterojunction under equilibrium is depicted in figure 2(d). Under forward and reverse bias, the band diagrams are shown in figures 2(e) and (f), respectively. As can be seen, under forward and reverse directions of bias, holes are able to

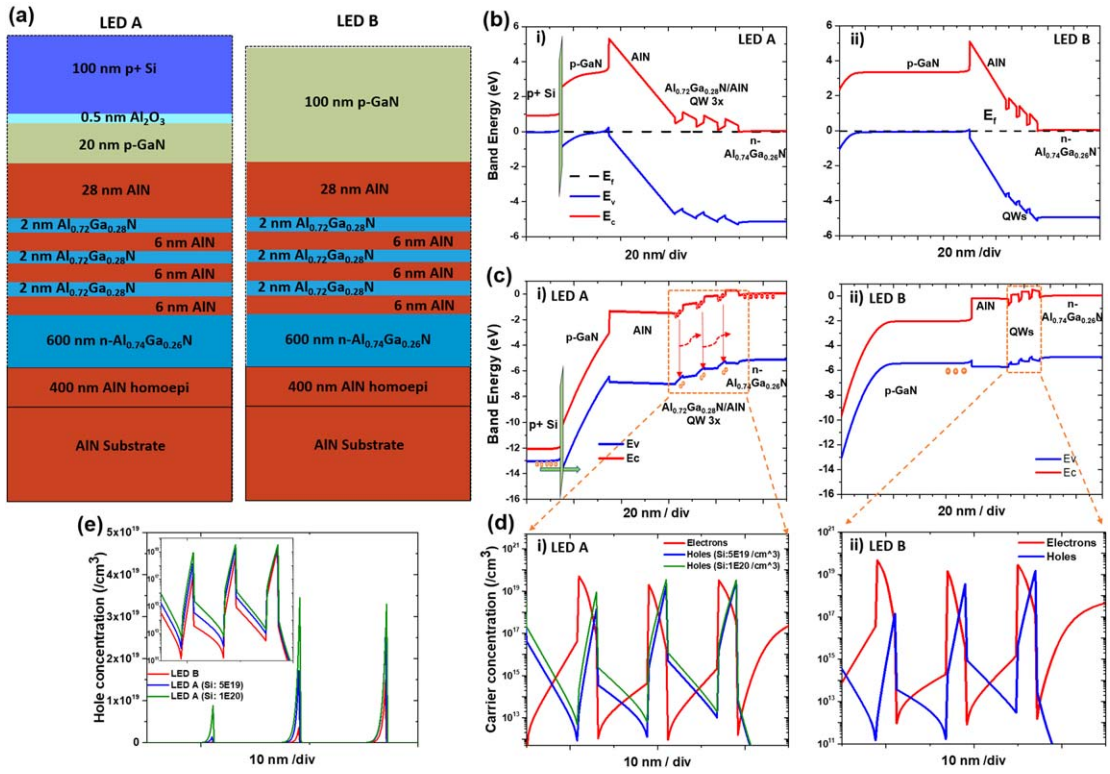


**Figure 3.** Electrical simulations of UVC LEDs examining the effects of p-Si/$Al_2O_3$/p-GaN heterojunction on hole injection. (a) Schematic illustration of two simulated LED structures. The two LED structures are identical, except that LED A consists of 100 nm p-Si, 0.5 nm $Al_2O_3$, and 20 nm p-GaN, and LED B only consists of 100 nm p-type GaN on their p-sides. (b) The band diagrams of (i) LED A and (ii) LED B under thermal equilibrium. (c) Band diagrams of (i) LED A and (ii) LED B under forward bias (driving current density: 100 A $cm^{-2}$). (d) Electron (red) and hole concentration (blue) distributions within the three QWs under forward bias for (i) LED A and (ii) LED B. In LED A, both the blue and green lines represent hole concentrations in the three QWs. The blue and green lines were obtained under hole concentrations of $5 \times 10^{19}$ $cm^{-3}$ and $1 \times 10^{20}$ $cm^{-3}$ in p-type Si, respectively. (e) Comparison of hole concentrations between LED A and LED B. LED A has much higher hole concentrations than LED B in the three QWs. The inset shows the plot in its logarithmic scale.

transport across the heterojunction via intra-band tunneling and thermal emission, respectively, leading to quasi-Ohmic *I*–*V* characteristics, as supported by the electrical measurements (figure 2(b)).

### 2.3. Effects of p-Si/$Al_2O_3$/p-GaN heterojunction on hole injection in UVC LEDs

To examine the effects of p-Si/$Al_2O_3$/p-GaN heterojunction on hole injection in UVC LEDs, two LED structures, shown in figure 3(a), were simulated using Silvaco®. Intra-band tunneling model was employed, and a polarization strength factor (a constant scale factor multiplied by the calculated spontaneous and piezoelectric polarization charges) of 0.4 was used in the simulations. There can be different types of screening effects to the field induced by polarization charge, which makes the scale factor smaller than 1 in most cases, such as ionization of dopant [27, 28]. The only difference between the two LED structures is their p-type sides: LED A has the p-Si/$Al_2O_3$/p-GaN heterojunction and the thickness of the p-type GaN layer is 20 nm, while LED B only has a 100 nm thick p-type GaN layer. After applying the band alignment of p-Si/$Al_2O_3$/p-GaN heterojunction as shown in figure 2(d), the band structures of LED A under zero bias (equilibrium) is plotted in figure 3(b)(i). For comparison, the band structure of LED B is plotted in figure 3(b)(ii). Figure 3(c) plots the band structures of the two LEDs under forward bias. As can be seen from figure 3(c)(i), the 20 nm p-type GaN in LED A is fully depleted and becomes a drift region for holes under forward bias. The strong internal electric field in the p-GaN layer, which caused the steep bending, is a combined effect of polarization and applied voltage. As a result, the 20 nm p-type GaN does not function as a hole injector in LED A, but rather a hole transport layer. In contrast, the 100 nm p-type GaN in LED B is only partially depleted and therefore is a hole supplier layer (figure 3(c)(ii)).

For LED A, under forward bias, the hole transport from the p-type Si into the p-type GaN became easier, as the triangular-shape energy barrier between the p-type Si and p-type GaN (0.97 eV) became narrower (~1 nm) than its equilibrium state (figure 3(b)(i)), as shown in figure 3(c)(i), to facilitate hole tunneling. The favorable overall energy band alignment enabled efficient hole transport from the p-type Si to the drift region, and further to the MQWs region.

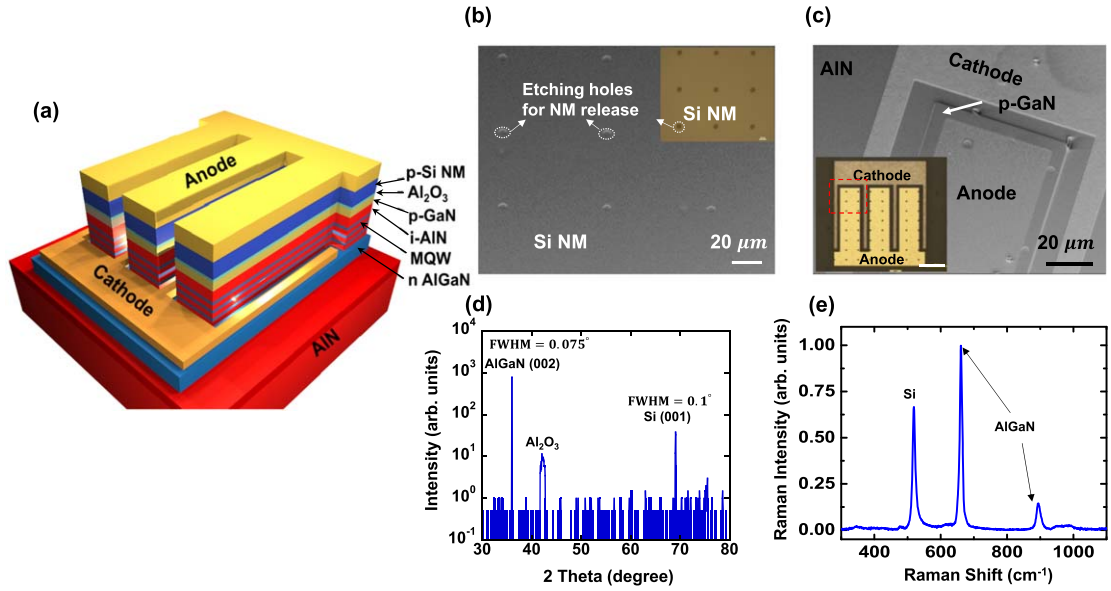


**Figure 4.** UVC LED with p-type Si as hole injector. (a) Three-dimensional illustration of an LED with a heavily doped p-type single-crystal Si NM as its hole injector. The anode metal is placed on top of the Si NM and the cathode metal is placed on top of the n-type $Al_{0.74}Ga_{0.26}N$ layer. (b) An SEM image of a p-type Si/$Al_2O_3$/p-type GaN structure: Si NM was transferred and bonded to $Al_2O_3$-coated p-type GaN. Inset: an optical microscope image of a piece of the Si NM. (c) An SEM image, corresponding to the red outlined area of the inset optical microscopic image, of a completed UVC LED with one anode finger between two cathode fingers. The scale bar is 20 $\mu$m and the device area is $1.31 \times 10^{-3}$ cm$^2$. (d) XRD data taken from a p-Si/$Al_2O_3$/p-GaN/p-GaN/i-AlN/$Al_{0.72}Ga_{0.28}N$ MQWs/n-$Al_{0.74}Ga_{0.26}N$/AlN structure. (e) Raman spectrum of the p-Si/$Al_2O_3$/p-GaN/i-AlN/$Al_{0.72}Ga_{0.28}N$ MQWs/n-$Al_{0.74}Ga_{0.26}N$/AlN structure.

The ample hole supply from the p-type Si and the efficient hole transport path led to a much higher hole density in the MQWs of LED A than in LED B and thus a more balanced electron/hole density in LED A (the blue line in figure 3(d)(i)) than LED B (figure 3(d)(ii)), even though the p-type Si was only doped to the level of $5 \times 10^{19}$ cm$^{-3}$. As the doping concentration of the p-type Si was increased to $1 \times 10^{20}$ cm$^{-3}$ (without changing any other LED parameters), the hole density in the MQWs of LED A further increased (the green line in figure 3(d)(i)). The increase in hole density in the MQWs following the increase in the hole concentration in the p-type Si furthermore verified that the p-type Si functioned as a hole supplier.

Figure 3(e) plots the direct comparison of hole densities between the two LEDs in linear scale with the inset showing a logarithmic scale plot. It is observed that the hole density in LED A, especially within the first two QWs, is significantly enhanced in comparison to LED B. The enhanced density of holes in the MQW is expected to enhance the electron–hole radiative recombination and therefore, the performance of UVC LEDs. The more holes that are present in the MQWs, the higher the recombination rate. Figure B1 shows the higher recombination rate when the hole concentration in the p-type Si is higher. It is noted that the p-type Si hole injector approach used in this work is readily applicable to UV LEDs covering a broad range of wavelengths.

### 2.4. Experimental application of p-type Si hole injector to UVC LEDs

The epitaxial layers of LED A (figure 3(a)) were grown on an AlN substrate by low pressure organometallic vapor phase epitaxy (LP-OMVPE) in a custom high-temperature reactor (see the SI for details of epitaxial growth). Two different LED samples have been grown that differ only by the thickness of the p-type GaN layer. The 20 nm Mg-doped p-type GaN layer here was grown, and also serves as a barrier layer to circumvent the rapid oxidation of the AlN surface (see figure C1 in the SI). The procedure to form the p-type Si hole injector via Si NM transfer and bonding is identical to that shown in figure 1. A detailed LED fabrication process flow is shown in figure D1 in the SI. The completed three-dimensional UVC LED structure is illustrated in figure 4(a). Figure 4(b) shows a scanning electron microscope (SEM) image of a piece of Si NM that was bonded to the epitaxial LED layer. Figure 4(c) shows an SEM image of a part of a fabricated UVC LED and the inset shows an optical image of a top view of the LED.

It is crucial to maintain strain-free bonding during the bonding process, since the strain in the Si NM can create unwanted band bending or even surface states at the interface. In figure 4(d), the x-ray diffraction (XRD) 2-theta-omega scan range from 30° to 80° at ~0.05° steps taken from the completed p-Si/$Al_2O_3$/p-GaN/i-AlN/i-$Al_{0.72}Ga_{0.28}N$/AlN MQWs/n-$Al_{0.74}GaN_{0.26}$/AlN structure shows three peaks corresponding to the AlGaN (002) direction, $Al_2O_3$ (002), and Si (001) directions, respectively. FWHM values of

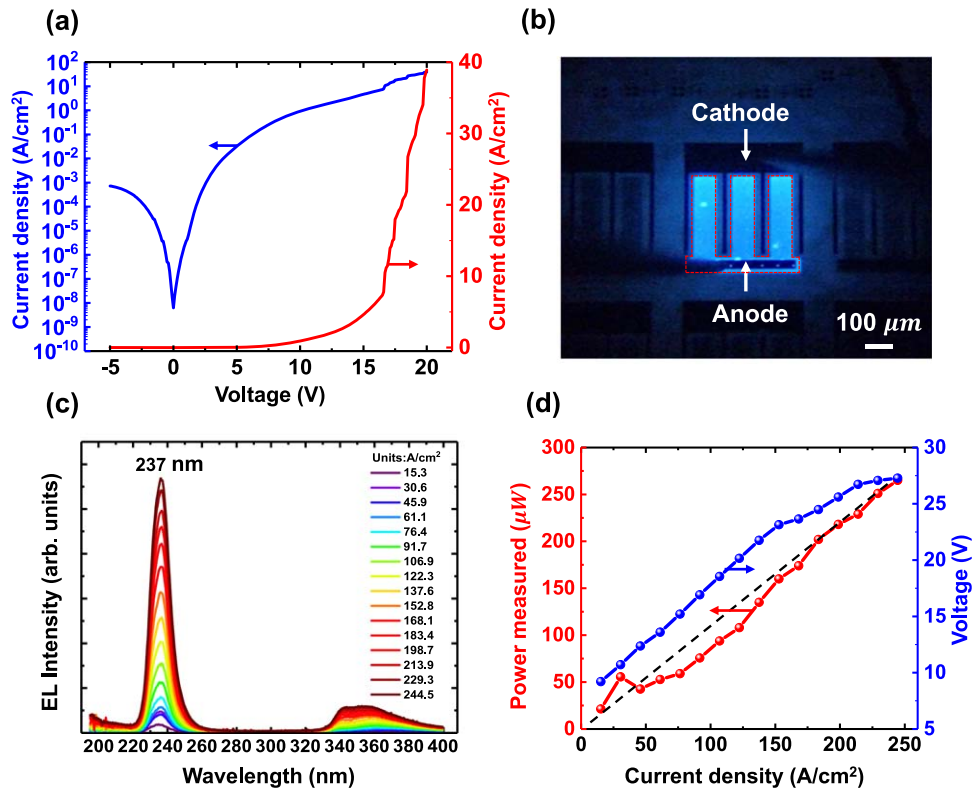


**Figure 5.** Measured electrical characteristics and electroluminescence performance of a UVC LED. (a) Measured current density–voltage characteristics of the fabricated UV LED. (b) An optical microscope image of the UV LED under bias with weak blue electroluminescence. (c) EL spectra (linear scale) taken at drive currents ranging from 20 to 320 mA. The main peak wavelength is 237 nm. (d) Measured light output power and the corresponding voltage applied to the LED versus current density applied. The dotted line was drawn to show the linear trend of the light output power.

0.075° and 0.1° from AlGaN and Si indicate that both the AlGaN epi-layer and transferred Si NM layer maintained good crystallinity during the transfer/bonding processes. The appearance of the weak $Al_2O_3$ peak at 42.1° in the XRD spectrum (figure 4(d)) indicates the existence of crystalline $Al_2O_3$, which may be attributed to the re-crystallization of the ALD interfacial $Al_2O_3$ during the annealing process. The weak intensity and the wide FWHM is attributed to the small thickness and may also imply that the ALD deposited $Al_2O_3$ was only partially crystallized, which is consistent with the HRTEM image shown in figure 2(a). To evaluate the strain of the Si/AlN/AlGaN heterostructure, Raman spectroscopy was carried out using a Horiba LabRAM ARAMIS Raman confocal microscope equipped with a 50× objective lens and a monochromator that has a 1000 mm focal length with an f/8 aperture. The spectrometer resolution is 0.045 $cm^{-1}$ and the laser spot size is about 1 $\mu$m. The power of the 532 nm green excitation line (lexc) is 18.5 mW. As shown in figure 4(e), the Raman characteristic peak for Si nanomembrane [29] that is taken from the Si/AlN/AlGaN heterostructure appeared at 521 $cm^{-1}$, indicating that the transfer-printed Si nanomembrane layer did not experience any strain due to the bonding process. Also, the two phonon modes which appeared around 660 $cm^{-1}$ ($E_2$(high) mode) and 900 $cm^{-1}$ ($A_1$(LO) mode) implies that the top AlN electron barrier layer did not suffer from the built-in strain due to the lattice mismatch or different thermal expansion coefficient between the AlGaN [30] epi-layer and the substrate [31]. Overall, both the XRD results and Raman peak indicate that an extremely low strain and high crystal quality $Al_xGa_{1-x}N$ epi-layer was grown by using an AlN substrate. In addition, the transfer-printed Si nanomembrane layer does not create strain in AlGaN/AlN epi-wafer.

The measured current density–voltage ($J$–$V$) plot for the UVC LED (figure 5(a)) shows its rectifying characteristics. Figure 5(b) shows an optical image of an LED under forward bias with weak blue emission, most likely from the p-type GaN and deep levels elsewhere in the device, which is commonly reported in UVC LED literature [32, 33]. The linear scale of the electroluminescence (EL) spectra for various current densities from 15.3 to 244.5 A $cm^{-2}$ are depicted in figure 5(c), where the dominant emission peak appeared at 237 nm, which is from the $Al_{0.72}Ga_{0.28}N$/AlN MQWs. With the current densities ranging from 15.3 to 244.5 A $cm^{-2}$, the intensity of the 237 nm emission peak monotonically increases with increasing drive. Alongside the main peak emission, there is another rather weak parasitic peak detected in the near-UV range. The parasitic peak, likely from excitation by 237 nm photons of the top p-type GaN combined with deep-levels in AlGaN, is much weaker than that of the recently reported 232 nm UVC LED [7]. The measured light output power and applied voltage

versus the current density (*L–I–V*) of the LED is plotted in figure 5(d). It can be seen that the light output power increases linearly with current density up to 245 A $cm^{-2}$, which is equivalent to a current of 320 mA. This linear behavior implies an absence of efficiency droop in this range, which directly results from the use of p-type Si as the hole injector. The fairly balanced electron–hole density improves quantum efficiency in comparison to the conventional p-type GaN-based hole injectors [34]. Besides the efficiency droop-free behavior, 265 $\mu$W output power was measured from the UVC LED at a current density of 245 A $cm^{-2}$ with an external voltage bias of 27.3 V, corresponding to an external quantum efficiency of 0.016% and a wall-plug efficiency of 0.003%. The efficiency is presently limited by the use of the relatively thick 20 nm p-type GaN layer, which absorbs UVC light, and thick AlN layer (28 nm), both inducing unnecessary series resistance. The relatively large turn-on voltage is a result of the large resistance of the near intrinsic AlN electron blocking layer and the non-ohmic metal contact made on the n-type $Al_{0.74}Ga_{0.26}N$ layer. Further optimizations of the LED structures are expected to lead to better performances. While this is not the highest reported efficiency [33, 35], the results clearly indicate the advantages of using p-type Si as a hole injector given that our LED provides the high UVC output power under constant current mode, which includes self-heating effects. It is further noticed that the ultrathin oxide interfaced lattice-mismatched heterojunction approach is applicable to other combinations of materials for various applications [20].

## 3. Conclusion

In summary, using transferred p-type Si as the hole injector via the ultrathin oxide-interfaced large lattice-mismatched heterojunction approach proves to be a viable route toward overcoming the poor hole injection challenge of deep-UV LEDs. The wide applicability of the approach could enable many new III-nitride-based junction devices. Applying the approach to LEDs of shorter wavelengths and large LED arrays may be one of the directions of future research.

## Acknowledgement

The work was supported by Defense Advanced Research Projects Agency (DARPA) under Grant HR0011-15-2-0002 (PMs: Dr Daniel Green and Dr Young-Kai Chen).

## Competing interests

The authors declare no competing financial interests.

## Author contributions

SJC, DL, and J-HS contributed to the work equally. All performed the research. DL, BM, RD, JDA, SJC, KK, ZM, WZ, and J-HS interpreted the data and wrote the manuscript. DZ contributed to manuscript writing; JDA managed research progress. ZM designed the research.

## ORCID iDs

Sang June Cho https://orcid.org/0000-0002-7784-2498
Jung-Hun Seo https://orcid.org/0000-0002-5039-2503
Munho Kim https://orcid.org/0000-0002-0379-1886

## References

[1] Brochen S, Brault J, Chenot S, Dussaigne A, Leroux M and Damilano B 2013 Dependence of the Mg-related acceptor ionization energy with the acceptor concentration in p-type GaN layers grown by molecular beam epitaxy *Appl. Phys. Lett.* **103** 032102
[2] Nam K, Nakarmi M, Li J, Lin J and Jiang H 2003 Mg acceptor level in AlN probed by deep ultraviolet photoluminescence *Appl. Phys. Lett.* **83** 878–80
[3] Nakarmi M, Nepal N, Ugolini C, Altahtamouni T, Lin J and Jiang H 2006 Correlation between optical and electrical properties of Mg-doped AlN epilayers *Appl. Phys. Lett.* **89** 152120
[4] Nakarmi M, Nepal N, Lin J and Jiang H 2009 Photoluminescence studies of impurity transitions in Mg-doped AlGaN alloys *Appl. Phys. Lett.* **94** 091903

[5] Iveland J, Martinelli L, Peretti J, Speck J S and Weisbuch C 2013 Direct measurement of Auger electrons emitted from a semiconductor light-emitting diode under electrical injection: identification of the dominant mechanism for efficiency droop *Phys. Rev. Lett.* **110** 177406

[6] Simon J, Protasenko V, Lian C, Xing H and Jena D 2010 Polarization-induced hole doping in wide–band-gap uniaxial semiconductor heterostructures *Science* **327** 60–4

[7] Islam S, Lee K, Verma J, Protasenko V, Rouvimov S, Bharadwaj S, Xing H and Jena D 2017 MBE-grown 232–270 nm deep-UV LEDs using monolayer thin binary GaN/AlN quantum heterostructures *Appl. Phys. Lett.* **110** 041108

[8] Ambacher O, Foutz B, Smart J, Shealy J, Weimann N, Chu K, Murphy M, Sierakowski A, Schaff W and Eastman L 2000 Two dimensional electron gases induced by spontaneous and piezoelectric polarization in undoped and doped AlGaN/GaN heterostructures *J. Appl. Phys.* **87** 334–44

[9] Peng Z, Shi-Bin L, Hong-Ping Y, Zhi-Ming W, Zhi C and Ya-Dong J 2014 Polarization induced high Al composition AlGaN p–n junction grown on silicon substrates *Chin. Phys. Lett.* **31** 118102

[10] Zheng T, Lin W, Liu R, Cai D, Li J, Li S and Kang J 2016 Improved p-type conductivity in Al-rich AlGaN using multidimensional Mg-doped superlattices *Sci. Rep.* **6** 21897

[11] Jena D, Heikman S, Green D, Buttari D, Coffie R, Xing H, Keller S, DenBaars S, Speck J S and Mishra U K 2002 Realization of wide electron slabs by polarization bulk doping in graded III–V nitride semiconductor alloys *Appl. Phys. Lett.* **81** 4395–7

[12] Li S, Zhang T, Wu J, Yang Y, Wang Z, Wu Z, Chen Z and Jiang Y 2013 Polarization induced hole doping in graded $Al_xGa_{1-x}N$ ($x = 0.7\sim1$) layer grown by molecular beam epitaxy *Appl. Phys. Lett.* **102** 062108

[13] Neufeld C J, Cruz S C, Farrell R M, Iza M, Lang J R, Keller S, Nakamura S, DenBaars S P, Speck J S and Mishra U K 2011 Effect of doping and polarization on carrier collection in InGaN quantum well solar cells *Appl. Phys. Lett.* **98** 243507

[14] Sánchez-Rojas J, Garrido J and Munoz E 2000 Tailoring of internal fields in AlGaN/GaN and InGaN/GaN heterostructure devices *Phys. Rev.* B **61** 2773

[15] Kozodoy P, Smorchkova Y P, Hansen M, Xing H, DenBaars S P, Mishra U K, Saxler A, Perrin R and Mitchel W 1999 Polarization-enhanced Mg doping of AlGaN/GaN superlattices *Appl. Phys. Lett.* **75** 2444–6

[16] Li K, Liu X, Wang Q, Zhao S and Mi Z 2015 Ultralow-threshold electrically injected AlGaN nanowire ultraviolet lasers on Si operating at low temperature *Nat. Nanotechnol.* **10** 140

[17] Xiang R, Fang Y-Y, Dai J, Zhang L, Su C, Wu Z, Yu C, Xiong H, Chen C and Hao Y 2011 High quality GaN epilayers grown on Si (1 1 1) with thin nonlinearly composition-graded $Al_xGa_{1-x}N$ interlayers via metal-organic chemical vapor deposition *J. Alloys Compd.* **509** 2227–31

[18] Hsu S and Liu C 2006 Fabrication of thin-GaN LED structures by Au–Si wafer bonding *Electrochem. Solid-State Lett.* **9** G171–3

[19] Ma Z and Seo J-H 2014 Lattice mismatched heterojunction structures and devices made therefrom *US Patent* No 8,866,154

[20] Liu D *et al* 2018 Lattice-mismatched semiconductor heterostructures arXiv:1812.10225v1

[21] Liu D, Cho S J, Park J, Seo J-H, Dalmau R, Zhao D, Kim K, Gong J, Kim M and Lee I-K 2018 229 nm UV LEDs on aluminum nitride single crystal substrates using p-type silicon for increased hole injection *Appl. Phys. Lett.* **112** 081101

[22] Hezel R and Jaeger K 1989 Low-temperature surface passivation of silicon for solar cells *J. Electrochem. Soc.* **136** 518–23

[23] Hoex B, Heil S, Langereis E, Van de Sanden M and Kessels W 2006 Ultralow surface recombination of c-Si substrates passivated by plasma-assisted atomic layer deposited $Al_2O_3$ *Appl. Phys. Lett.* **89** 042112

[24] Hashizume T, Ootomo S, Inagaki T and Hasegawa H 2003 Surface passivation of GaN and GaN/AlGaN heterostructures by dielectric films and its application to insulated-gate heterostructure transistors *J. Vac. Sci. Technol.* B **21** 1828–38

[25] Wang H, Chung J W, Gao X, Guo S and Palacios T 2010 $Al_2O_3$ passivated InAlN/GaN HEMTs on SiC substrate with record current density and transconductance *Phys. Status Solidi* c **7** 2440–4

[26] Sze S M and Ng K K 2006 *Physics of Semiconductor Devices* (New York: Wiley)

[27] Di Carlo A, Della Sala F, Lugli P, Fiorentini V and Bernardini F 2000 Doping screening of polarization fields in nitride heterostructures *Appl. Phys. Lett.* **76** 3950–2

[28] Della Sala F, Di Carlo A, Lugli P, Bernardini F, Fiorentini V, Scholz R and Jancu J-M 1999 Free-carrier screening of polarization fields in wurtzite GaN/InGaN laser structures *Appl. Phys. Lett.* **74** 2002–4

[29] Kim M, Mi H, Cho M, Seo J-H, Zhou W, Gong S and Ma Z 2015 Tunable biaxial in-plane compressive strain in a Si nanomembrane transferred on a polyimide film *Appl. Phys. Lett.* **106** 212107

[30] Kirste R, Mohn S, Wagner M R, Reparaz J S and Hoffmann A 2012 Phonon plasmon interaction in ternary group-III-nitrides *Appl. Phys. Lett.* **101** 041909

[31] Davydov V Y, Goncharuk I, Smirnov A, Nikolaev A, Lundin W, Usikov A, Klochikhin A, Aderhold J, Graul J and Semchinova O 2002 Composition dependence of optical phonon energies and Raman line broadening in hexagonal $Al_xGa_{1-x}N$ alloys *Phys. Rev.* B **65** 125203

[32] Liu X, Mou Y, Wang H, Liang R, Wang X, Peng Y and Chen M 2018 Enhanced light extraction of deep ultraviolet light-emitting diodes by using optimized aluminum reflector *Appl. Opt.* **57** 7325–8

[33] Hirayama H, Fujikawa S and Kamata N 2015 Recent progress in AlGaN-based deep-UV LEDs *Electron. Commun. Japan* **98** 1–8

[34] Verma J, Kandaswamy P K, Protasenko V, Verma A, Grace Xing H and Jena D 2013 Tunnel-injection GaN quantum dot ultraviolet light-emitting diodes *Appl. Phys. Lett.* **102** 041103

[35] Hirayama H, Noguchi N, Yatabe T and Kamata N 2008 227 nm AlGaN light-emitting diode with 0.15 mW output power realized using a thin quantum well and AlN buffer with reduced threading dislocation density *Appl. Phys. Express* **1** 051101